Fuel 304 (2021) 121403

Contents lists available at ScienceDirect

Fuel

journal homepage: www.elsevier.com/locate/fuel

Experimental and kinetic study of NO-reburning by syngas under high CO_2 concentration in a jet stirred reactor

Fan Hu [a], Pengfei Li [a,b,*], Wenhao Li [a], Cuijiao Ding [a], Junjun Guo [a], Zhaohui Liu [a]

[a] State Key Laboratory of Coal Combustion, School of Energy and Power Engineering, Huazhong University of Science and Technology, Wuhan 430074, China
[b] China Coal Research Institute, China Coal Technology and Engineering Group, Beijing 100013, China

ARTICLE INFO

Keywords:
NO-reburning
Syngas
Jet-stirred reactor (JSR)
CO_2 dilution
Methane addition

ABSTRACT

The NO-reburning by syngas is investigated by the jet-stirred reactor (JSR) experiments and kinetic modeling. The effects of CO_2 and methane are studied systematically under different reaction temperatures (T), equivalence ratios (Φ) and initial ratios of hydrogen to carbon monoxide (α). The kinetic modeling is carried out by the present modified detailed mechanism consisting of 151 species and 1408 reactions. The modeling results obtained using the present modified mechanism demonstrate the good consistency with experiments under most of the conditions. The CO_2 has significant inhibitory effect on the NO-reburning by syngas independent of variations in T, Φ and α. The maximum NO reduction efficiency is remarkably reduced than that under N_2 condition by at least 76%. The addition of 1000 ppm methane has been found to increase the NO-reburning by the syngas for CO_2 conditions by at least 243%. The effects of CO_2 and CH_4 must be considered for NO-reburning by syngas as the actual syngas contains CO_2 and methane. Considering the presence of CO_2 and CH_4, the optimal condition to maximize the NO reduction efficiency is $T \approx 1150$ K, $\Phi \approx 1.67$ and $\alpha \approx 1$. The mechanism under this optimal condition is determinate by pathway and sensitivity analyses. The critical reactions for NO-reburning by syngas in the presence of CO_2 and CH_4 are identified, which are important for future mechanism development and application of NO-reburning by syngas.

1. Introduction

With the increasingly stringent emission standards of nitrogen oxides, controlling the NO_x emissions from the combustion process has become an essential concern of the international combustion community [1,2]. Reburning is an inexpensive and high-efficiency NO_x reduction technology that has been widely used in the combustion application [3–5]. The NO_x emission can be reduced by 35%–65% through NO-reburning based on different furnaces and combustion conditions [3]. Natural gas, liquefied petroleum gas, pulverized coal, and biomass have been used as reburning fuels [4]. Recently, synthesis gas or syngas, which is a clean energy resource and regarded as a promising fuel to substitute traditional fossil energy in the immediate future [6,7], is also considered to be a reburning fuel.

The NO-reburning by syngas has been investigated in flow reactors [8–10], bench-scale systems [11], and pilot-scale furnaces [12–14]. Glarborg et al. [8] examined the NO-reduction by non-hydrocarbon fuels in a flow reactor. They found that an increase in the content of CH_4 can enhance the NO-reburning by non-hydrocarbon fuels. Dagaut et al. [9] studied the NO reduction using gases obtained from biomass pyrolysis in a jet-stirred reactor (JSR). They found that the NO reduction by the mixture of CO and H_2 is very poor and the addition of hydrocarbon mixture can increase the NO reduction. Werle et al. [10] numerically investigated the NO-reburning by sewage sludge-derived syngas by a plug-flow reactor (PFR). Their calculations presented an optimum temperature of 1200 K in the NO-reburning. Zhao et al. [15] reported that the NO reduction effect can be enhanced by increasing the initial NO concentration under fuel-rich conditions in PFR. In general, the syngas composition includes the combustible matter of H_2, CO, and CH_4, and adequate amounts of diluents of N_2 and CO_2 [6,16]. Most previous studies considered the syngas as H_2/CO, which has been extensively investigated in respects of the ignition delay time [17], flame speed [18], extinction limit [19], and NO_x emissions [20]. Recently, some scholars found that the presence of CH_4 and CO_2 in actual syngas has a dramatic influence on reactions. Mathieu et al. [21] found that the ignition delay time can be noticeably increased with the

* Corresponding author at: State Key Laboratory of Coal Combustion, School of Energy and Power Engineering, Huazhong University of Science and Technology, Wuhan 430074, China.
E-mail address: pfli@hust.edu.cn (P. Li).

https://doi.org/10.1016/j.fuel.2021.121403
Received 7 February 2021; Received in revised form 29 June 2021; Accepted 6 July 2021
Available online 15 July 2021
0016-2361/

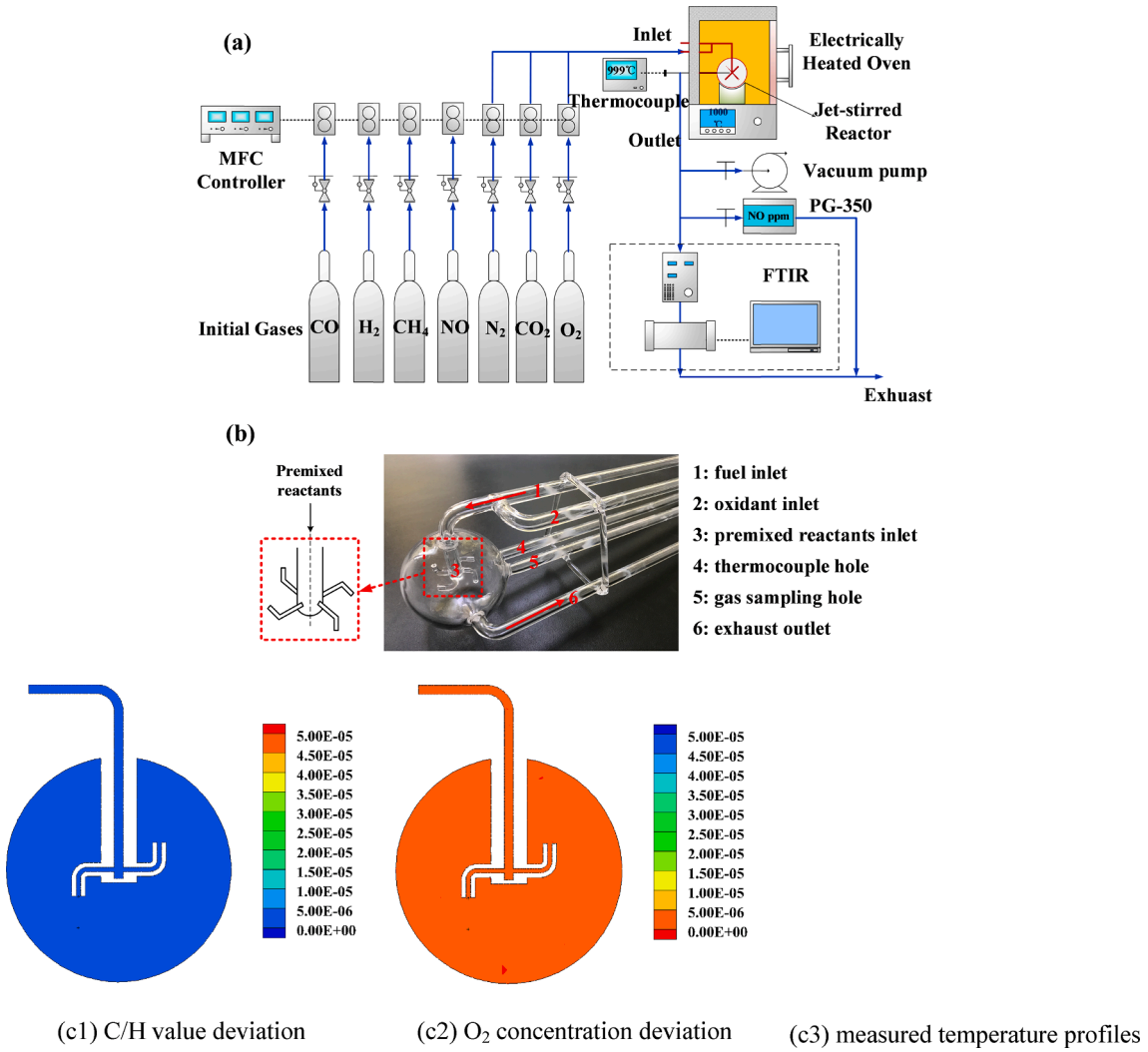

Fig. 1. Schematic diagram of the present jet-stirred reactor (JSR) experimental system (a) flow chart of the experimental system, (b) schematic diagram of the JSR, and (c) uniformity of the reactor: deviation distributions between CFD simulations and the theoretical values (c1) C/H value and (c2) O_2 concentration; (c3) measured temperatures in the transverse direction of the JSR.

Table 1
Experimental conditions of the present syngas NO-reburning study.

Case	Φ	Inlet Streams CO ppm	H_2 ppm	CH_4 ppm	NO ppm	O_2 vol %	CO_2 vol %	T/K
1	0.5, 1, 1.67	5000	5000	0	1000	1, 0.5, 0.3	0	***600–1350***
2	0.5, 1, 1.67	5000	5000	0	1000	1, 0.5, 0.3	30	***600–1350***
3	***0.5–2.5***	5000	5000	0	1000	1–0.2	0	1100, 1200, 1300
4	***0.5–2.5***	5000	5000	0	1000	1–0.2	30	1100, 1200, 1300
5	0.5–2.5	***2000***	***8000***	0	1000	1–0.2	0	1100, 1200, 1300
6	0.5–2.5	***2000***	***8000***	0	1000	1–0.2	30	1100, 1200, 1300
7	0.5–2.5	***8000***	***2000***	0	1000	1–0.2	0	1100, 1200, 1300
8	0.5–2.5	***8000***	***2000***	0	1000	1–0.2	30	1100, 1200, 1300
9	0.5, 1, 1.67	4500	4500	***1000***	1000	1.3, 0.65, 0.39	0	***600–1350***
10	0.5, 1, 1.67	4500	4500	***1000***	1000	1.3, 0.65, 0.39	30	***600–1350***
11	0.5–2.17	4500	4500	***1000***	1000	***1.3–0.3***	0	1100, 1200, 1300
12	0.5–2.17	4500	4500	***1000***	1000	***1.3–0.3***	30	1100, 1200, 1300

addition of CH_4. Wang et al. [22] concluded that the impact of H_2 level on flame speed is decreased as increasing the CO_2 level. Wang et al. [23] discovered that diluting with CO_2 can reduce more NO emission than the diluting with N_2. It is worth noting that the above previous studies on the NO-reburning by syngas do not consider the presence of both CO_2 and CH_4. For actual syngas, there must be plenty of CO_2 and may be a certain amount of CH_4. Therefore, it is necessary to examine the effects of CO_2 and CH_4 on NO-reburning by syngas.

As the actual syngas contains CH_4, the NO-reburning by hydrocarbon fuels also needs to be reviewed. Dagaut et al. [24–26] systematically investigated NO reburning by a variety of gaseous fuels (C1–C4) in N_2 atmosphere by experiments and kinetic modeling in a JSR. They found

Table 2
Nine detailed mechanisms with nitrogen chemistry.

Mechanism	Species	Reactions	References
PG2018	151	1397	Glarborg et al., [54]
GRI-Mech 3.0	53	325	Smith et al., [55]
GRI-Mech 2.11	49	277	Bowman et al., [56]
KONNOV	129	1231	Konnov, [57]
PG2009	97	778	Mendiara and Glarborg, [58]
DAGAUT	147	1087	Dagaut and Nicolle, [51]
POLIMI	115	2141	CRECK, [59]
USC-GRI2.11	111	784	Wang et al. [60], Bowman et al., [56]
PG2018-mod	151	1408	present modified

that increasing reaction temperature can strengthen the formation of thermal NO and the maximum NO reduction at a given temperature is obtained in the slightly fuel-rich atmosphere. Biabao et al. [27] discussed the impact of temperature on NO reburning by natural gas in a PFR and their results show that increasing temperature can enhance NO reburning from 1473 K to 1773 K under the O_2/N_2 atmosphere. Do et al. [28] experimentally examined the NO reburning effect by biomass pyrolysis gases in a drop-tube reactor and they found the NO reduction is positively related to reaction temperature from 1073 K to 1273 K under O_2/N_2 conditions. Nicolle et al. [29] numerically concluded that the reactions of NO converted to HCN and NH_3 are very active prior to auto-ignition during NO-burning in MILD combustion of CH_4 with N_2 as the bath gas. Liesa et al. [30] examined the impact of H_2O on NO reburning by CH_4 in a flow-reactor experimentally using N_2 as the carrier gas. They found that the H_2O can reduce the consumption of CH_4 and NO and restrain the generation of CO and HCN, while promotes the generation of H_2. Wang et al. [31] also drew the conclusion that water vapor inhibits the NO reduction by CH_4. Gimenez-Lopez et al. [32] found that the NO reduction effect by CH_4 can be enhanced by increasing the initial NO concentration. Shu et al. [33] investigated pyrolysis gases from different biomass in the tubular reactor with the balance gas as N_2 and they found that the CH_4 plays the most important role in NO reburning processing, while CO and H_2 play relatively minor roles. The above studies indicate that the previous studies on NO-reburning were mainly carried out using hydrocarbon (C1–C4, especially methane) as reburning fuels in the O_2/N_2 atmosphere. The investigation on NO-reburning under CO_2 conditions is limited.

In order to achieve the goal of "carbon neutrality", the carbon capture, utilization, and storage (CCUS) technology is the key strategic development direction [34]. There are two very important parts in CCUS: capture and utilization. For utilization, the chemical utilization (e.g., synthesizing dimethyl ether [35]), the physical utilization (e.g., CO_2 enhanced oil recovery [36]), and bio-utilization (e.g., the nitrifier-enriched activated sludge approach [37,38]) are the main routes. For capture, the pre-combustion (e.g., integrated gasification combined cycle [39]), post-combustion [40], and the oxy-fuel combustion [41,42] are very important and mainstream technologies, among which, the oxy-fuel combustion is regarded as one of the most potential technologies for large-scale carbon capture [43].

The NO-reburning is also important for suppressing the NO_x emission under oxy-fuel conditions [44]. The previous studies in the CO_2 atmosphere are mainly carried out in the zero-dimensional JSR [45] or one-dimensional PFR [32,46,47] using the hydrocarbon as fuels. Mendiara et al. [46] investigated the NO reburning by methane in PFR under N_2 and CO_2 conditions and discussed the influences of temperature and equivalence ratio. Their results displayed that the NO reduction effect of methane is at the considerable level under the fuel-rich condition no matter in N_2 or CO_2 atmosphere, while under $\Phi \leq 1$ conditions, the NO reduction in CO_2 atmosphere is higher than that in N_2 atmosphere. Normann et al. [48] found that NO reburning effect in CO_2 atmosphere is more sensitive to the reaction temperature and less influenced by equivalence ratio. This is mainly caused by that the high concentration CO_2 affects the oxidation process of hydrocarbons and enhances the importance of CH_3 in NO reduction process. Kühnemuth et al. [49] experimentally examined the NO reburning by propane in a 100-kW furnace in the atmosphere of N_2 and CO_2. Their results show that the NO reburning effect in CO_2 atmosphere is lower than that in N_2 atmosphere, while for considering the recirculation effect of flue gas, the total NO reduction in CO_2 atmosphere is higher than that in N_2 atmosphere. Li et al. [45] systematically investigated NO reduction by methane in a JSR under both N_2 and CO_2 conditions. They reported that the maximum NO reduction occurs at $T = 1300$ K and $\Phi = 1.25$ in CO_2 atmosphere, while for $T > 1100$ K, the NO reburning effect under CO_2 conditions is decreased by 40%–60% in comparison to that under N_2 conditions. To sum up, there are few studies on the NO-reburning by gaseous fuels under oxy-fuel combustion conditions, let alone related studies involving syngas.

From the above literature review, to the best of our knowledge, there are no systematic kinetic studies on NO-reburning by syngas under oxy-fuel combustion atmosphere. The JSR is a kind of ideal zero-dimensional continuous stirred reactor, which is very suitable for investigating gaseous chemical kinetics [29,50]. The JSR exhibits extreme uniform distributions of temperature and gas compositions due to the high-speed jets of the JSR nozzles. Therefore, the reactions in the JSR take place in a nearly homogeneous condition, and they can be the approximate representation of the local reaction at a specific space point [51,52]. Hence, it is necessary to systematically study the effects of different factors on NO-reburning by syngas under oxy-fuel conditions in a JSR, especially the effects of methane and CO_2 addition. This paper is designed for closing the gap. Specifically, the objective of the present work is to investigate the NO-reburning by syngas systematically through JSR experiments and kinetic modeling. This is the first study to investigate the NO-reburning by syngas in the presence of both CO_2 and CH_4. The effects of CO_2 and CH_4 are examined in detail under different reaction

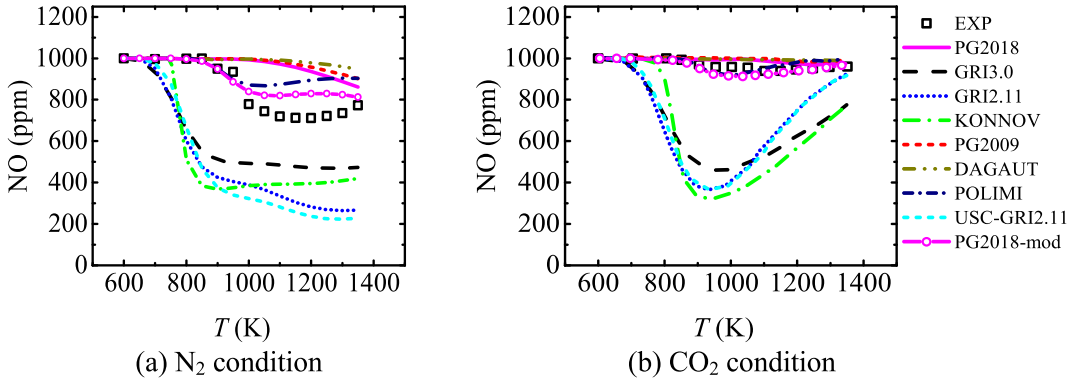

Fig. 2. Optimization of the detailed kinetic mechanism (a) $\Phi = 1.67$, $X_{CO} = 5000$ ppm, $X_{H2} = 5000$ ppm, $X_{NO} = 1000$ ppm, (b) $\Phi = 1.67$, $X_{CO} = 5000$ ppm, $X_{H2} = 5000$ ppm, $X_{NO} = 1000$ ppm, $X_{CO2} = 0.30$.

Table 3
Parameter information for the updated chemical reactions.

No.	reaction	A	β	E_a	reference	remark
1	$CO + HO_2 \leftrightarrow CO_2 + OH$	1.57E + 5	2.18	17,940	[61]	modified
2	$CO + OH \leftrightarrow CO_2 + H$	7.015E + 4	2.053	−355.7	[62]	modified
3	$CO_2 + NH \leftrightarrow HNO + CO$	1.36E-10	0	34,500	[63]	added
4	$HNCO + OH \leftrightarrow CO_2 + NH_2$	1.54E-14	1.5	3597	[64]	added
5	$HOCHO + OH \leftrightarrow H_2O + CO_2 + H$	2.62E + 6	2.06	916	[65]	added
6	$HOCHO + H \leftrightarrow H_2 + CO_2 + H$	4.24E + 6	2.1	4868	[65]	added
7	$HCOH + O_2 \leftrightarrow CO_2 + H_2O$	1E + 13	0	0	[66]	added
8	$HCOH + O_2 \leftrightarrow CO_2 + OH + H$	1E + 13	0	0	[66]	added
9	$CH_3 + NO (+M) \leftrightarrow CH_3NO(+M)$	2.17E + 8	0.6	0	[67]	modified
10	$CH_3O + NO (+M) \leftrightarrow CH_3ONO(+M)$	1.21E + 10	0	0	[68]	modified
11	$CH_4 + NO \leftrightarrow HNO + CH_3$	5E + 8	0	50,032	[69]	added
12	$CH_2 + NO \leftrightarrow H + HNCO$	3.1E + 17	−1.38	1270	[55]	added
13	$CH_2(S) + NO \leftrightarrow H + HNCO$	3.1E + 17	−1.38	1270	[55]	added
14	$CH_2 + NO \leftrightarrow NCO + H_2$	3.5E + 9	0	−1090	[70]	added
15	$CH_2(S) + NO \leftrightarrow NCO + H_2$	3.5E + 9	0	−1090	[70]	added
16	$NH + NO \leftrightarrow N_2O + H$	1.8E + 14	−0.4	−244	[71]	modified
17	$NH + NO \leftrightarrow N_2 + OH$	2.7E + 12	−0.1	−512	[71]	modified
18	$H + NO + M \leftrightarrow HNO + M$	4E + 20	−1.75	0	[59]	modified
19	$H_2NO + M \leftrightarrow HNO + H + M$	1E + 16	0	50,000	[59]	modified
20	$H_2NO + H \leftrightarrow NH_2 + OH$	5E + 13	0	0	[59]	modified
21	$H_2NO + O \leftrightarrow NH_2 + O_2$	2E + 14	0	0	[59]	modified
22	$NH_2 + NO \leftrightarrow NNH + OH$	8.9E + 12	−0.35	0	[59]	modified
23	$NH_2 + NO \leftrightarrow N_2 + H_2O$	1.72E + 19	−2.294	1058	[59]	modified
24	$NNH \leftrightarrow N_2 + H$	1E + 7	0	0	[59]	modified

temperatures (T), equivalence ratios (Φ), and the initial ratios of hydrogen to carbon monoxide (α). A detailed mechanism is modified and updated for the present kinetic modeling.

2. Experimental details

2.1. Experimental facility

The experiments are carried out in an in-house made jet-stirred reactor (JSR) system (Fig. 1). Fig. 1a illustrates the flow chart of the experimental system, including the sub-systems of reaction gas supply, heating furnace, JSR and measurement. The schematic diagram of the JSR is displayed in Fig. 1b, which contains a 50-mm diameter fused-silica sphere designed with four 1-mm diameter nozzles. The orientation of each nozzle is different, so the direction and speed of the mixed gas at the nozzle outlet can ensure that the gas is fully and evenly mixed in the reactor, reaching nearly perfect mixing. In the experiments, the fuels are premixed with NO and sent into the JSR via the inlet 1, while the oxygen and the diluted gases N_2 or CO_2 are premixed and brought into the JSR via the inlet 2 in Fig. 1b. The inner diameters of inlets 1 and 2 are both 2 mm. Seen in Fig. 1b, there is a premixed and preheated chamber for reactants, whose length and volume are approximately 10 cm and 0.3 cm^3, respectively. The reaction of the reactants in this zone is negligible, resulting from the residence time there is about 1/200 of that in the JSR.

According to David et al. [52] in Nancy, the design criteria of the JSR are: (1) the jets from four nozzles must be turbulent, (2) the four nozzles must provide intense internal recirculation to ensure good mixing, and (3) the jet velocity at the nozzle exit shouldn't exceed the speed of sound. Through the derivation of theoretical formulas, the first and third criteria determine the achievable residence time range (as shown in Eq. (1)), and the second criteria determine the geometric ratio between the inner diameters of the reactor and the nozzle (as shown in Eq. (2)).

$$\frac{4}{3}\frac{R^3}{d^2 c_{sound}} \leqslant \tau \leqslant \frac{\rho A R^3}{230 \eta d} \tag{1}$$

$$A\frac{R}{d} > 19 \tag{2}$$

where R and d denote the radius of the reactor and the diameter of the nozzle, respectively, c_{sound} is the speed of sound, τ is the residence time, A is an adimensionnal constant, and ρ and η are specific weight and dynamic viscosity of the gas, respectively.

For the verification of the present JSR using the above criteria, the gas flowing into the reactor is assumed to be the mixture of 70% N_2 and 30% CO_2 (vol.) at the temperature of 723 K with the constant flow of 1 NL/min. The R and d are 0.025 m and 0.001 m, respectively. At 723 K, the ρ and η of the mixture are 0.6 kg•m^{-3} and 3.4 × 10^{-5} Pa•s, respectively, and the constant A is $4/\pi$. The upper and lower limits of residence time calculated from Eq. (1) are 0.04 s and 1.53 s. For the present experiment, the typical mean residence time at 723 K is approximately 1.36 s, which is in the range of residence time. Then, as $A\frac{R}{d} \approx 31.8 > 19$, the present JSR meets the second criteria. To sum up, the JSR used in this paper complies with the design criteria.

The verification results of the reactor uniformity are shown in Fig. 1c. To confirm the degree of mixing, CFD simulation of the present reactor is conducted applying the realizable k-ε model with the aid of ANSYS Fluent. Fig. 1(c1)–1(c2) display the deviation distributions between CFD simulations and the theoretical values of C/H value and O_2 concentration. The results of species in Fig. 1(c1) and 1(c2) reveal that the deviations are<0.0006%. Fig. 1 (c3) shows the measured temperature distribution in the transverse direction of the JSR. It's displayed that the deviation value of temperature is<7 K, regardless of there is fuel or there is no reaction. Therefore, the present reactor is well-mixed and it can be regarded as a perfectly stirred reactor.

2.2. Measurement details

The reaction temperature of the JSR is regulated by the temperature control system of the electric heated oven. At the same time, an S-type thermocouple (Pt-10%Rh-Pt) is applied to record the internal temperature of the reactor, with error limit less than ± 0.25%. During present experiments, high purity gases (99.99%) are supplied by high pressure cylinders and their flow is regulated by the mass flowmeter and flow controller. The portable Fourier transform infrared spectroscopy (FTIR, Gasmet-DX4000) and HORIBA PG-350 gas analyzer are used for on-line measurement of the gas components. The FTIR, whose resolution and scanning speed are set at 8 cm^{-1} and 10 scans/s, can simultaneously measure the concentrations of CH_4, O_2, CO_2, NO, CO, HCN, NO_2, and N_2O components with errors less than ± 1%. Before the experiments, the calibration of the FTIR is conducted by using various given concentrations of single gases at various temperatures. The concentration of O_2, CO_2, NO, and CO are also measured by the HORIBA PG-350, and the accuracies of which are O_2 (±1%, 0–25%), CO_2 (±2%, 0–30%), NO (1%, 0–5000 ppm) and CO (±5%, 0–4000 ppm). The measured values of both

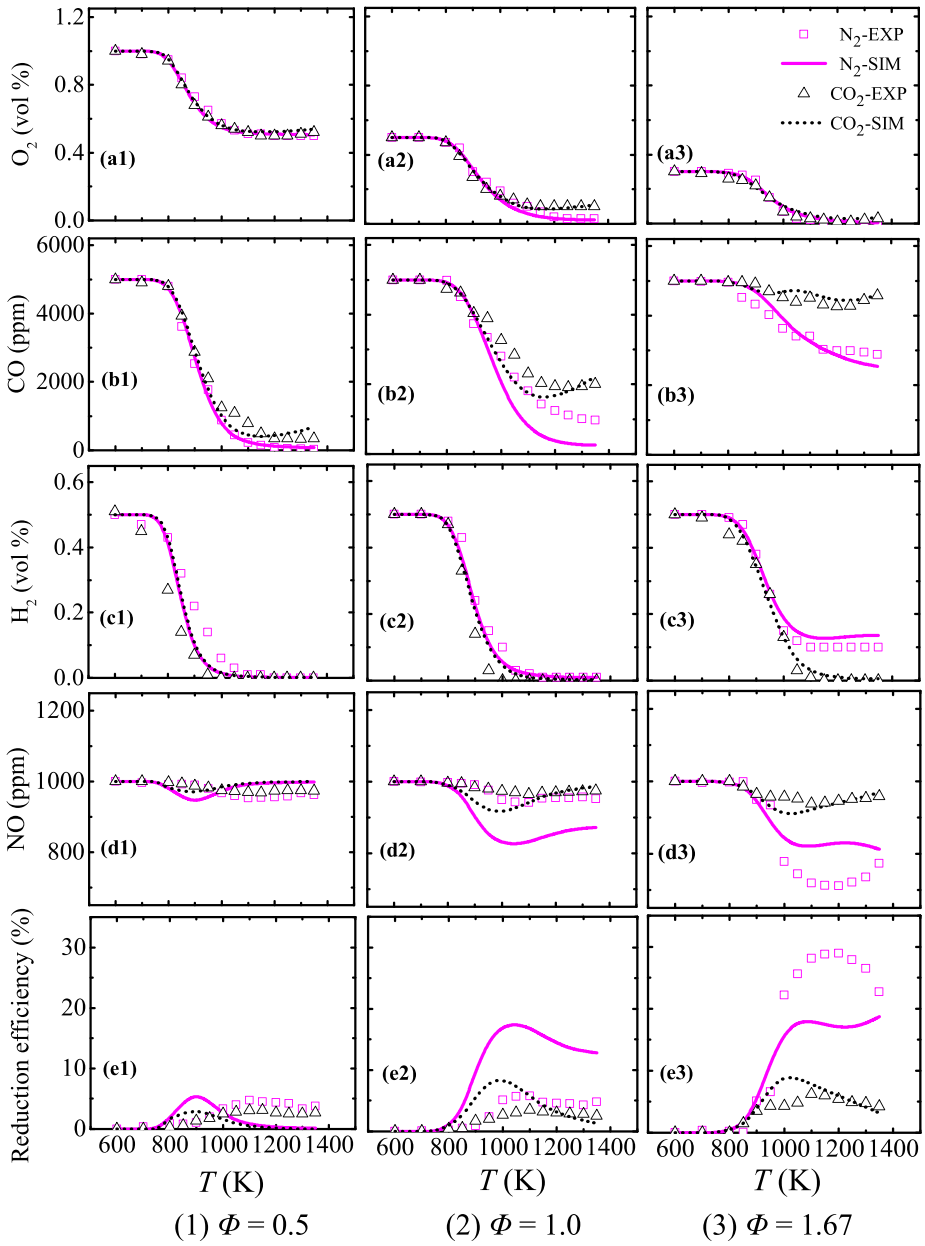

Fig. 3. Experimental and simulated concentrations of O_2, CO, H_2, NO, and NO reduction efficiency with different T under three Φ.

the PG350 and FTIR agree well.

2.3. Experimental conditions

In the present experiments, the total flow rate is controlled at 1 NL/min and the concentration of fuel gas is kept at 10000 ppm and the initial concentration of NO is maintained at 1000 ppm. The specific cases are shown in Table 1. Cases 1–8 are used to study the effect of CO_2 under different T (Cases 1–2), Φ (Cases 3–4) and α (Cases 3–8), respectively. The N_2 atmosphere is used as reference. The impact of methane addition at various T and Φ under N_2 and CO_2 atmospheres are investigated in Cases 9–12.

3. Kinetic modeling

The perfectly stirred reactor code [53] is applied for the chemical kinetics analysis and the transient solver is applied for all the experimental conditions. Simulations are performed isothermal conditions. Table 2 summarizes the commonly used and freely available detailed mechanisms: (1) PG2018 [54], (2) GRI3.0 [55], (3) GRI2.11 [56], (4) KONNOV [57], (5) PG2009 [58], (6) DAGAUT [51], (7) POLIMI [59], (8) USC-GRI2.11 (USC-Mech II [60] merged with the N mechanism from GRI-Mech 2.11), (9) PG2018-mod (present modified mechanism based on PG2018).

The PG2018 [54] and PG2009 [58] mechanisms are proposed by the group of Peter Glarborg in 2018 and 2009, respectively. They are mainly proposed to simulate the oxidation and nitrogen chemistry of C1 hydrocarbons under oxy-fuel conditions. The GRI3.0 [55] and GRI2.11 [56] mechanisms are widely used mechanisms for methane combustion in air. KONNOV [57] mechanism is a detailed mechanism for small hydrocarbon fuels with updated reactions of prompt-NO route. DAGAUT [51] mechanism is proposed by group of Philippe Dagaut to simulate NO-reburning by C1 to C4 hydrocarbon fuels and H_2/CO. POLIMI [59] mechanism is a detailed mechanism for modeling the pyrolysis, partial oxidation and combustion of C1 to C3 hydrocarbons with NO_x formation. USC-Mech II [60] mechanism is usually applied for modeling the

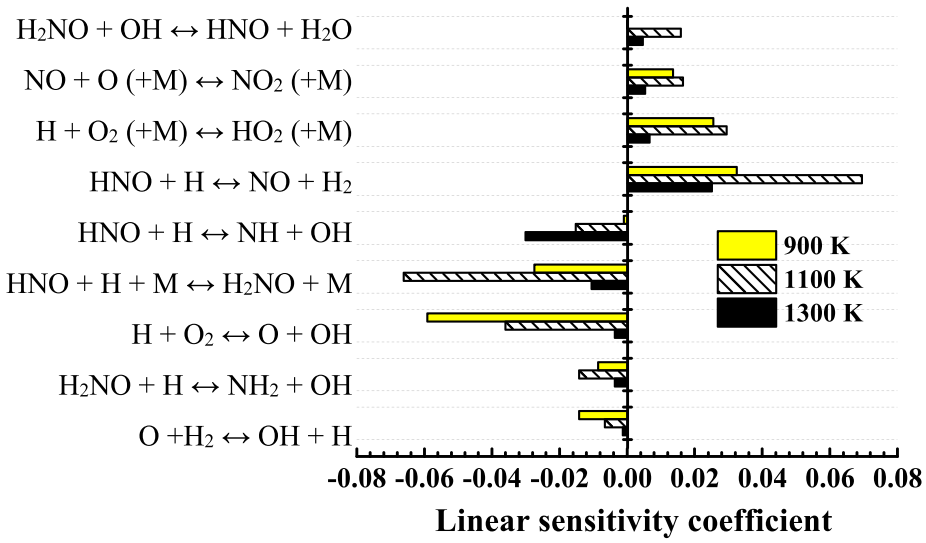

Fig. 4. First-order sensitivity analysis for NO formation and reduction of syngas at various reaction temperatures under CO_2 condition ($\Phi = 1.67$, $X_{CO} = 5000$ ppm, $X_{H2} = 5000$ ppm, $X_{NO} = 1000$ ppm, and $X_{CO2} = 0.30$).

combustion of C1-C4 hydrocarbon fuels and H_2/CO, and it is merged with N sub-mechanism from GRI-Mech 2.11.

For components such as CO, CO_2, O_2, and H_2, the calculated results of these nine detailed mechanisms are in good agreement with the experimental results, while there is a big difference for the NO concentration prediction. In order to better match the simulation results with the experimental results, the PG2018 mechanism is used as the basis, and some modifications and updates are made. The modification work is aimed at the reactions with vital impact on the NO reduction and formation under high CO_2 conditions. 24 reactions involving CO_2 and NO are updated or added through literature investigation, mechanism comparison, sensitivity analysis (SA) and rate of production (ROP). There are two aspects of modification: (1) important reactions involving CO_2, especially the main paths between CO and CO_2; (2) vital reactions of NO reduction by fuel mixture (CH_4, H_2 and CO).

For aspect (1), some modifications and optimization should be performed to consider the effect of high CO_2 concentration. First, reaction No.1 $CO + HO_2 \leftrightarrow CO_2 + OH$ [61] and No.2 $CO + OH \leftrightarrow CO_2 + H$ [62] have been found as the vital reactions for CO and CO_2 conversion and they have been updated by previous studies. Second, reactions No.3–8 [63–66] have been added to the modified mechanism, which are not contained in the original mechanism while play important role in the atmosphere of O_2/CO_2. For aspect (2), first, it is noted that the reduction of NO by CH_4 is mainly through CH_x radicals. The crucial reactions No.9 $CH_3 + NO$ (+M) $\leftrightarrow CH_3NO$ (+M) [67] and No.10 $CH_3O + NO$ (+M) $\leftrightarrow CH_3ONO$ (+M) [68] have been updated by previous studies, and reaction No. 11–15 [55,69,70] of NO reduction through CH_x radicals not considered in the initial mechanism has been added. Second, the reduction of NO by the mixture of CO and H_2 is mainly through the following path: $NO \rightarrow HNO \rightarrow NH_2 \rightarrow N_2$. Based on our experiments and considering the previous literature, we have modified and optimized the most sensitive reactions under the studied conditions in this paper such as $H + NO + M \leftrightarrow HNO + M$ [59], $NH_2 + NO \leftrightarrow N_2 + H_2O$ [59], and reaction No.16–17 [71], 19–22 [59], 24 [59].

It can be found from Fig. 2 that the results calculated by the present modified mechanism (PG2018-mod) are more consistent with the experimental data than other detailed mechanisms. Detailed modifications and updates of chemical reactions are listed in Table 3. The present PG2018-mod mechanism (whose mechanism file is available in supplementary material) consists of 151 species and 1408 reactions and is applied for all the modelling in this study.

The robustness of the modified mechanism is pretty good. The modified mechanism (PG2018-mod) can not only be applied to the reaction kinetics simulation, but also be used to predict the actual furnace reburning technology by properly simplifying the mechanism and performing computational fluid dynamics (CFD) simulation. Both the reliability of calculation results and the stability of calculation process are good. Methods to simplify and apply the mechanism to CFD can refer to our previous studies [72,73].

4. Results and analysis

4.1. Effect of reaction temperature

Experiments with two kinds of reactants (H_2-CO-NO-N_2 and H_2-CO-NO-CO_2) are performed in the JSR at 600–1350 K under fuel-lean ($\Phi = 0.5$), stoichiometric ($\Phi = 1.0$) and fuel-rich ($\Phi = 1.67$) conditions (Cases 1–2). H_2-CO-NO-N_2 and H_2-CO-NO-CO_2 denote the experimental conditions of syngas reaction with the addition of 1000 ppm NO in the N_2 and CO_2 atmosphere, respectively. Fig. 3 demonstrates the experimental (symbols) and simulated (lines) results of (a) O_2, (b) CO, (c) H_2 and (d) NO concentrations and (e) NO reduction efficiency as a function of reaction temperature (T) under three equivalence ratios ($\Phi = 0.5$, 1, and 1.67). It can be found that the calculated results by the present PG2018-mod mechanism are highly consistent with the experimental data for most conditions. As shown in Fig. 3, for both N_2 and CO_2 atmospheres, the oxidation reaction of syngas starts at around 700 K, and with the increase of temperature, CO and H_2 constantly transform and tend to be stable. At $T > 850$ K, the CO concentrations in CO_2 atmosphere are greater than that in N_2 atmosphere, while the H_2 concentrations are less than that in N_2 atmosphere. Thissuggests that the addition of CO_2 is beneficial to the conversion of H_2 while inhibits the conversion of CO. The reason is that the presence of high concentration of CO_2 promotes the forward process of reaction $CO_2 + H \leftrightarrow CO + OH$, inhibiting the oxidation process of CO to CO_2, and thus making more O_2 react with H_2 to enhance the conversion process of H_2.

Fig. 3d display the experimental and simulated results of the concentrations of NO with dependency on temperature. As shown in Fig. 3d, the simulations agree well with the experiments for most cases. In the cases of three Φ, the variation trends of NO are similar with the increase of T. Specifically, in the low-temperature section (600–800 K), NO concentrations remain the same. As T further increases, the NO concentration first drops to a certain extent and then stays the same. Under fuel-rich condition, the downtrend of NO concentration is the strongest. Under high CO_2 atmosphere, the decline of NO is distinctly weaker than that under N_2 atmosphere at $T > 900$ K.

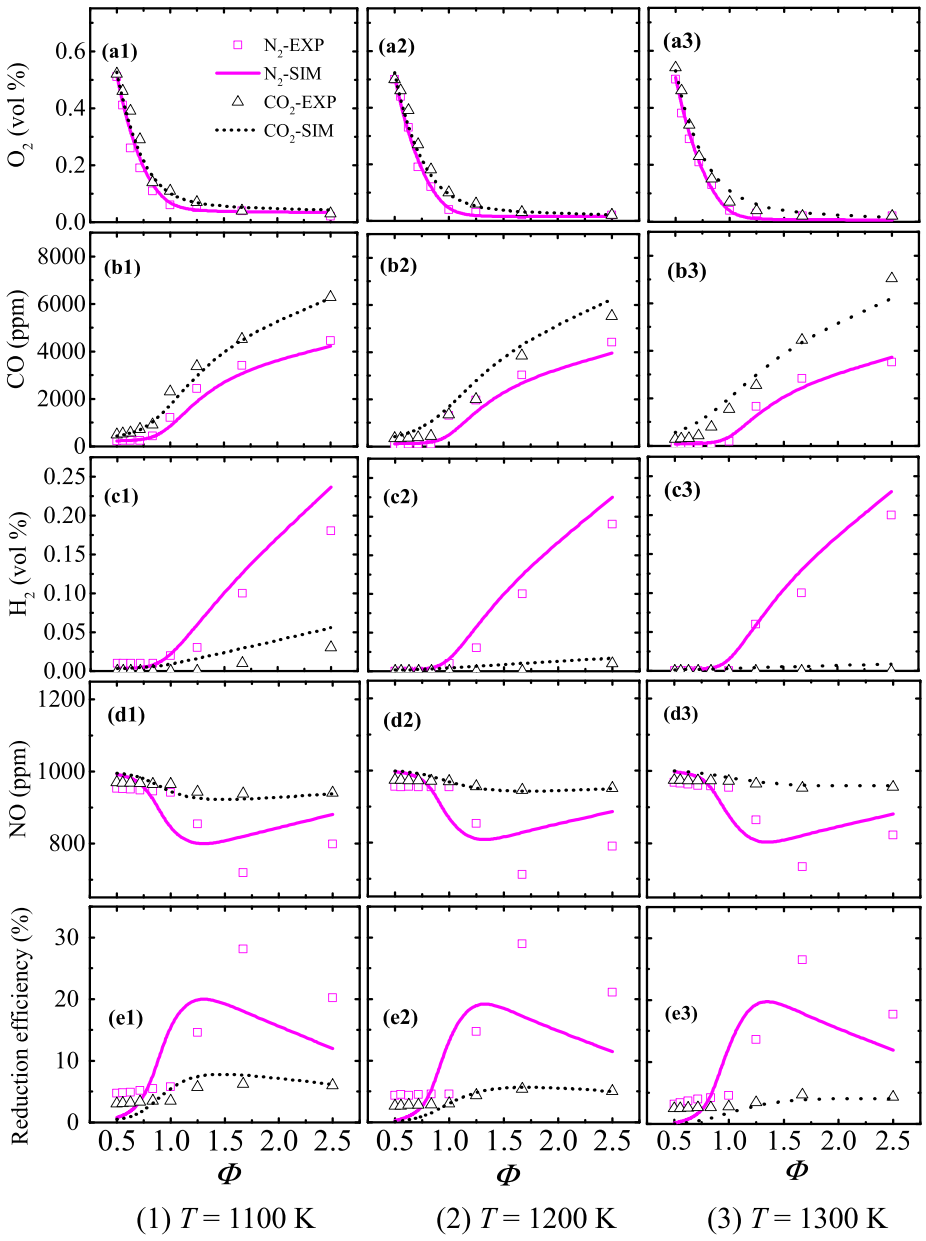

Fig. 5. Experimental and simulated results of O_2, CO, H_2, NO concentrations and NO reduction efficiencies with different Φ under three T.

To further quantitatively demonstrate the NO-reburning, Fig. 3e show the relationship between NO reduction efficiency and reaction temperature. The NO reduction efficiency is defined as: NO Reduction Efficiency (%) = 100% × (IFN–TFN) / IFN, where the IFN (initial fraction of N) and TFN (total fraction of N) denote the mole fraction of NO initially added and the sum of the mole fractions of NO and HCN, respectively. Based on the results in Fig. 3e, the NO reduction efficiency is basically zero in the low temperature section, indicating that there is no NO-reburning effect in this temperature range. With a further increase of T, the NO reduction efficiency of syngas first goes up and then decreases slightly.

Under fuel-lean and stoichiometric conditions (Φ = 0.5 & 1.0), experiments in Fig. 3(e1) & 3(e2) demonstrate that the differences of NO reduction efficiency between N_2 and CO_2 conditions are not apparent, although it's relatively weaker under CO_2 condition. The maximal NO reduction efficiency of 6% occurs at near 1100 K. Under fuel-rich condition (Φ = 1.67), under N_2 condition, the maximal NO reduction appears at T = 1150 K with the maximum NO reduction efficiency is about 29%, and the further increase of temperature is not conducive to NO reduction. While under CO_2 condition, the NO-reburning effect is inhibited significantly. There is an optimal temperature (about 1150 K) to maximize the NO reduction and with further increase of T has negative effect on reburning. The maximum NO reduction efficiency under CO_2 condition is<7%, which is reduced by 76% compared with that under N_2 condition. The results in the Fig. 3e indicate that the presence of high concentration CO_2 has significant influence on the NO-reburning by the syngas.

Fig. 4 exhibits the first-order sensitivity analysis for NO formation and reduction of syngas under the three temperatures in CO_2 atmosphere. It's found that, at 900 K and 1100 K, the most important reactions for promoting NO reduction are $H + O_2 \leftrightarrow O + OH$ and $HNO + H + M \leftrightarrow H_2NO + M$. The former reaction, as the main chain branching of oxidation reaction, is the key reaction to promote the oxidation of H_2 to H radical, and the importance of this reaction decreases as the increase of temperature. The latter reaction promotes the NO to HNO and further to H_2NO. At 1300 K, the most crucial reaction for NO reduction is HNO

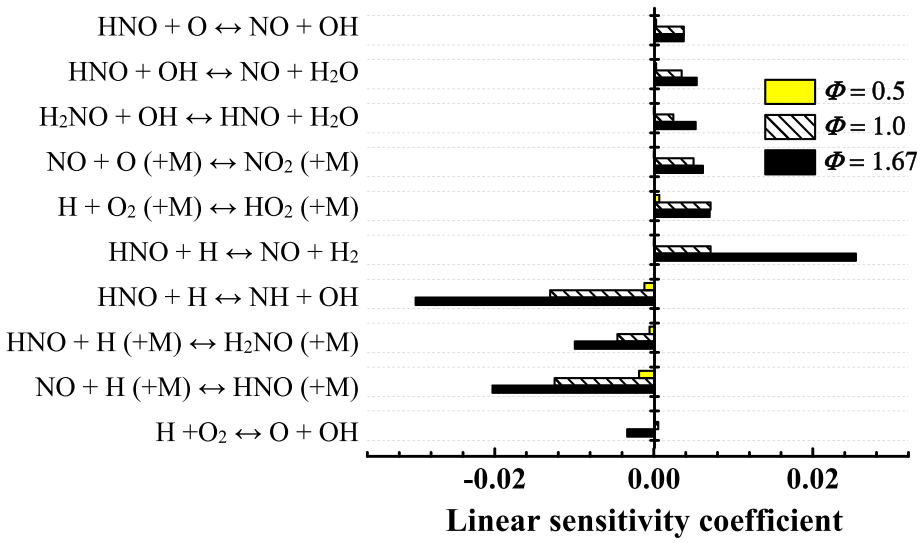

Fig. 6. First-order sensitivity analysis for NO of syngas at various Φ under CO_2 condition (T = 1300 K, X_{CO} = 5000 ppm, X_{H2} = 5000 ppm, X_{NO} = 1000 ppm, and X_{CO2} = 0.30).

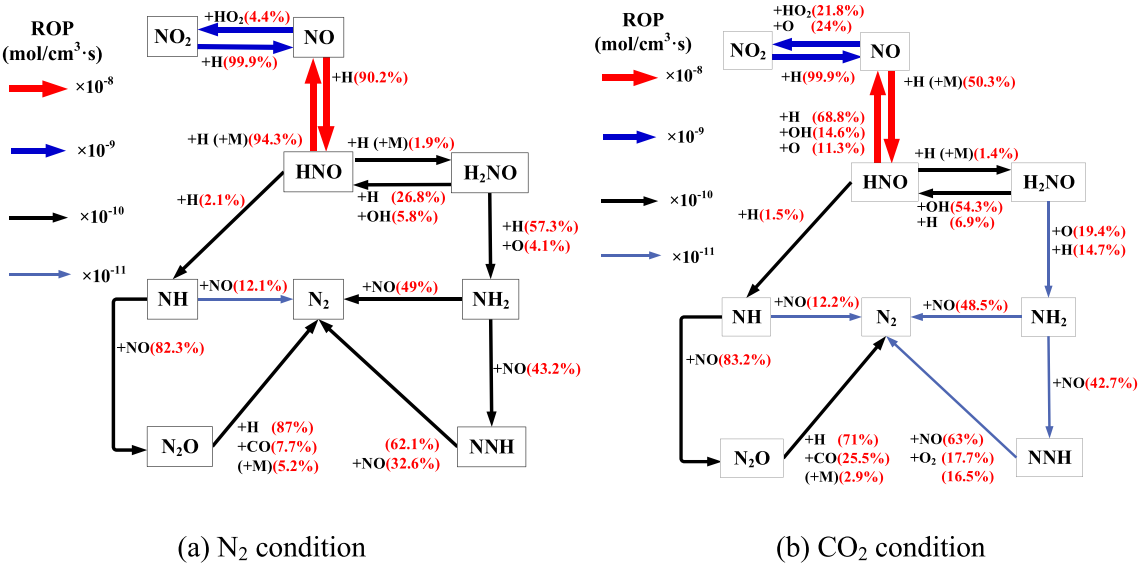

(a) N_2 condition (b) CO_2 condition

Fig. 7. Reaction pathways of NO reduction by syngas under (a) N_2 (T = 1300 K, Φ = 1.67, X_{CO} = 5000 ppm, X_{H2} = 5000 ppm, and X_{NO} = 1000 ppm) and (b) CO_2 (T = 1300 K, Φ = 1.67, X_{CO} = 5000 ppm, X_{H2} = 5000 ppm, X_{NO} = 1000 ppm, and X_{CO2} = 0.30) conditions.

+ H ↔ NH + OH, which indicates that HNO is more inclined to convert to NH and then to N_2 to achieve NO reduction as the increase of temperature. In addition, the most important reactions to inhibit the NO reduction are HNO + H ↔ NO + H_2 and H + O_2 (+M) ↔ HO_2 (+M). The former reaction inhibits the NO reduction by promoting HNO into NO, while the latter reaction promotes the HO_2 formation and then enhances the conversion of NO to NO_2.

4.2. Effect of equivalence ratio

The experimental and simulated results of (a) O_2, (b) CO, (c) H_2 and (d) NO concentrations and (e) NO reduction efficiency by syngas with dependency on equivalence ratio at three different temperatures (1100 K, 1200 K and 1300 K) are demonstrated in Fig. 5. The numerical results agree well with the experiments for most cases, especially under the high CO_2 concentration conditions. As shown in Fig. 5b and 5c, the CO and H_2 concentrations in CO_2 atmosphere are greater and less than that in N_2 atmosphere, respectively, and this phenomenon becomes more obvious with the increase of Φ. The results are consistent with that in Fig. 3b and 3c, which further indicates that the addition of CO_2 enhances the H_2 conversion while weakens the CO conversion.

Fig. 5d and 5e display the experiments and simulations of the concentrations of NO and the reduction efficiency with different Φ at 1100 K, 1200 K and 1300 K under the N_2 and CO_2 conditions (Cases 3–4). For the three T, the variation trends of NO are similar with increasing the equivalence ratios for both the N_2 and CO_2 atmospheres. Under N_2 condition, as Φ increases, the NO concentration first remains the same ($\Phi < 1$), and then decreases ($1 < \Phi < 1.67$), and finally increases slightly ($\Phi > 1.67$). Under the CO_2 condition, with the increase of Φ, the NO concentration remains the same first ($\Phi < 1$), and then drops to a certain level and then does not change significantly. The descending trend of NO under high concentration CO_2 condition is prominently lower than that in the N_2 atmosphere at fuel-rich condition $\Phi > 1$.

Fig. 5e indicate the NO reduction efficiency with various Φ. The NO reduction efficiency is about 3%–5% for both the N_2 and CO_2 conditions at $\Phi < 1$, signifying that under the fuel-lean condition, the NO-reburning

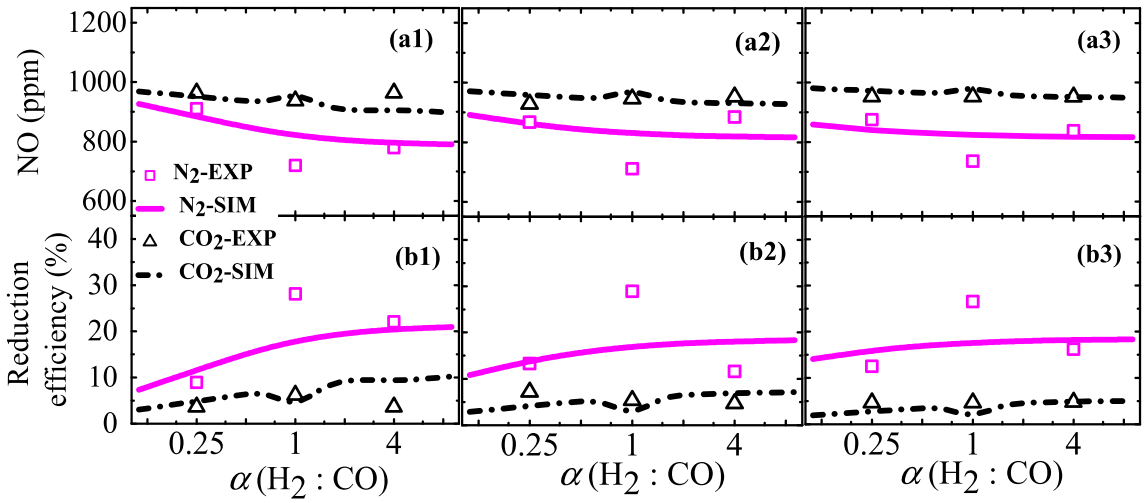

Fig. 8. Experimental and simulated results of NO concentration and NO reduction efficiencies with different α under $\Phi = 1.67$ for three T (a1) & (b1) $T = 1100$ K, (a2) & (b2) $T = 1200$ K, and (a3) & (b3) $T = 1300$ K.

effect by syngas is not obvious and is insensitive to reaction atmosphere. With a further increase of Φ, the NO reduction efficiency first increases and then decreases for the three reaction temperatures. For $\Phi > 1.0$, the difference between N_2 and CO_2 conditions in Fig. 6(e1) − 6(e3) is very obvious. Under the N_2 condition, the optimal Φ is about 1.67 with the maximum NO reduction efficiency of 29% and the further increase of Φ will weaken the NO-reburning. However, for CO_2 condition, the optimal Φ is also about 1.67 with the maximum NO reduction efficiency of only 6%. The maximum NO reduction efficiency is significantly lower than that under the N_2 condition by approximately 79%. Moreover, the further increase of Φ can't improve the NO-reburning by syngas under the CO_2 condition. Therefore, Fig. 5d and 5e indicate again that CO_2 has an significant effect on the NO-reburning by syngas at different Φ, and the optimal Φ for the maximum NO reduction efficiency is approximately 1.67, regardless of the N_2 or CO_2 atmosphere.

The first-order sensitivity analysis for NO formation and reduction of syngas under various Φ in CO_2 atmosphere is shown in Fig. 6. At these three temperatures, the most important reactions to promote NO reduction are HNO + H ↔ NH + OH, NO + H (+M) ↔ HNO (+M) and HNO + H (+M) ↔ H_2NO (+M), all of which are critical reactions for NO reduction. The most vital reactions to inhibit NO reduction are HNO + H ↔ NO + H_2 and H + O_2 (+M) ↔ HO_2 (+M). The former reaction promotes the conversion of HNO to NO and thus inhibits the NO reduction, while the latter reaction increases the HO_2 generation and then the conversion of NO to NO_2.

To further analyze the NO-reburning under various conditions, the detailed pathways of NO reduction by syngas are performed under the fuel-rich ($\Phi = 1.67$) condition at 1300 K in both N_2 and CO_2 atmospheres with the normalized reaction rate of production. As found in Fig. 7a, the paths of NO → HNO → H_2NO → NH_2 (→NNH) → N_2 and NO → HNO → NH → N_2O → N_2 are the primary pathways for NO reduction by syngas in N_2 atmosphere. The H radical occupies a vital role in the process of NO reduction, and 90.2% of NO is converted to HNO through the reaction with H radical. For CO_2 atmosphere as demonstrated in Fig. 8b, the main pathways of NO reduction are basically the same as that in N_2 atmosphere, while the whole reaction rate is somewhat reduced. Specifically, it can be found that the reaction path of NO → HNO → H_2NO → NH_2 (→NNH) → N_2 is significantly inhibited, and the reaction rate of related reactions is decreased by an order of magnitude in comparison with that in N_2 atmosphere. The reaction path of NO → HNO → NH → N_2O → N_2 is the critical path for NO reduction by syngas in CO_2 atmosphere. Furthermore, due to the decrease of H radical formation in CO_2 atmosphere, NO is more inclined to react with HO_2 to convert to NO_2 and then to NO again. The proportion of NO → HNO is only 50.3%, which is significantly reduced compared with 90.2% in N_2 atmosphere. Moreover, as the increase of OH radical generation in CO_2 atmosphere, the ratio of H_2NO to HNO is increased from 32.6% (N_2 atmosphere) to 61.2%, and the reaction path of NO → HNO → H_2NO → NH_2 (→NNH) → N_2 is weakened. Therefore, the NO reduction of syngas under CO_2 condition is observably lower than that under N_2 condition.

According to the reaction pathway analysis (Fig. 7), the paths of NO → HNO → H_2NO → NH_2 (→NNH) → N_2 and NO → HNO → NH → N_2O → N_2 are the primary pathways for NO reduction. The H radical plays a significant role in the process of NO reduction, and a large proportion of NO (90.2% for N_2 atmosphere and 50.3% for CO_2 atmosphere) is converted to HNO through the reaction with H radical. Therefore, the H_2 conversion has the priority.

4.3. Effect of the initial ratio of hydrogen to carbon monoxide

The experiments and simulations with dependency on α are shown in Fig. 8 (Cases 3–8). The simulations in Fig. 8 agree well with the experiments for most cases, especially under the high CO_2 concentration conditions. For the three T, the variation trends of NO, as demonstrated in Fig. 8a, are similar with the increase of α for both the N_2 and CO_2 conditions. Under N_2 condition, as the α increases, the NO concentration first decreases and then increases slightly, with the minimum NO obtained at $\alpha \approx 1$. However, under the CO_2 condition, the NO concentration remains the same with the increase of α.

Fig. 8b display the results of the NO reduction efficiency with various α. For the N_2 condition, the NO reduction efficiency first increases and then decreases as the α increases, and the maximum NO reduction efficiency is about 30% with the optimal $\alpha \approx 1$. However, for the CO_2 condition, the results are different, that is, the NO reduction efficiency basically has no obvious change (≈ 5%) as α increases. Importantly, the NO reduction efficiency under the CO_2 condition is notably decreased by 83% compared with that under the N_2 condition. The results in Fig. 8 indicate that the initial ratio of H_2 to CO has little effect on the NO-reburning of syngas, and the NO reduction efficiency cannot be significantly improved only by adjusting α.

4.4. Effect of addition of methane

As demonstrated in Figs. 3, 5, and 8, the NO-reburning by syngas is significantly inhibited under CO_2 condition (the maximum NO reduction efficiency < 10%) regardless of the variation of T, Φ and α. Considering that the actual syngas may contain a certain amount of methane, the effects of adding methane are discussed (Cases 9–12) in this section.

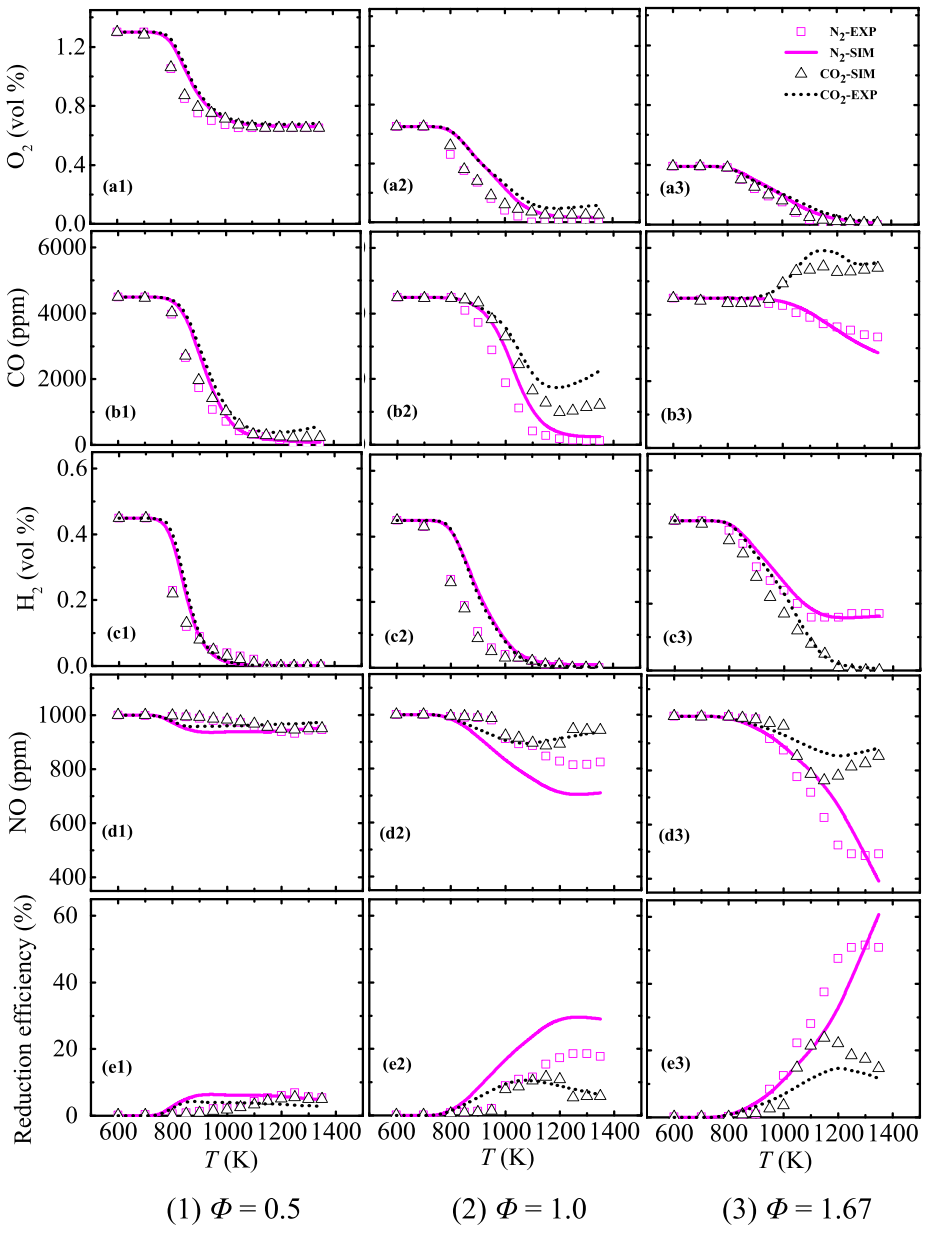

Fig. 9. Experimental and simulated results of O_2, CO, H_2, NO concentrations and NO reduction efficiencies with different T under three Φ with addition of methane.

Fig. 9 demonstrates the experimental and simulated results of O_2, CO, H_2, and NO concentrations and NO reduction efficiency by syngas with methane addition as a function of T under three Φ. The simulation results can well repeat the experimental trends, and show good consistency with the experiments under most conditions. The oxidation process in Fig. 9a–9c is similar to that in Fig. 3a–3c without methane addition.

Fig. 9d display the experimental and simulated results of the concentrations of NO with dependency on temperature with 1000 ppm methane addition under fuel-lean (Φ = 0.5), stoichiometric (Φ = 1.0), and fuel-rich (Φ = 1.67) conditions. The variation trends of NO are similar with the increase of T at the three Φ cases for both the N_2 and CO_2 conditions. The general variations of NO are consistent with Fig. 3d, while the maximum decreases of NO are all greater than the corresponding reaction conditions in Fig. 3d. This shows that the addition of 1000 ppm methane can lead to the significant decrease of NO for both the N_2 and CO_2 atmospheres.

According to the results in Fig. 9e, under N_2 condition, the maximum NO reduction efficiency is about 52% at the temperature of 1300 K under fuel-rich condition, which is increased by 79% compared with the results in Fig. 3e in the absence of CH_4. Under the CO_2 condition, the reburning is still strongly inhibited in the presence of methane. The maximum NO reduction efficiency in Fig. 9e is approximately 24% occuring at the temperature of 1150 K, and it is significantly increased relative to the results in Fig. 3e by approximately 243%. The results in the Fig. 9e indicate that the addition of 1000 ppm methane can significantly improve the NO-reburning. Because the actual sgngas may contain CH_4, the NO-reburning can be improved by operating the reaction conditon at the optimal condition proposed by the present work.

The experimental and simulated results of O_2, CO, H_2, and NO concentrations and NO reduction efficiency by syngas with methane addition as a function of Φ under three T are displayed in Fig. 10. The numerical results by the present PG2018-mod mechanism are in good agreement with the experimental data for most cases, especially under CO_2 condition. As displayed in Fig. 10a–c, the oxidation process is analogous to the corresponding conditions in Fig. 5a–5c in the absence of methane.

Fig. 10d & 10e exhibit the concentrations of NO and the reduction

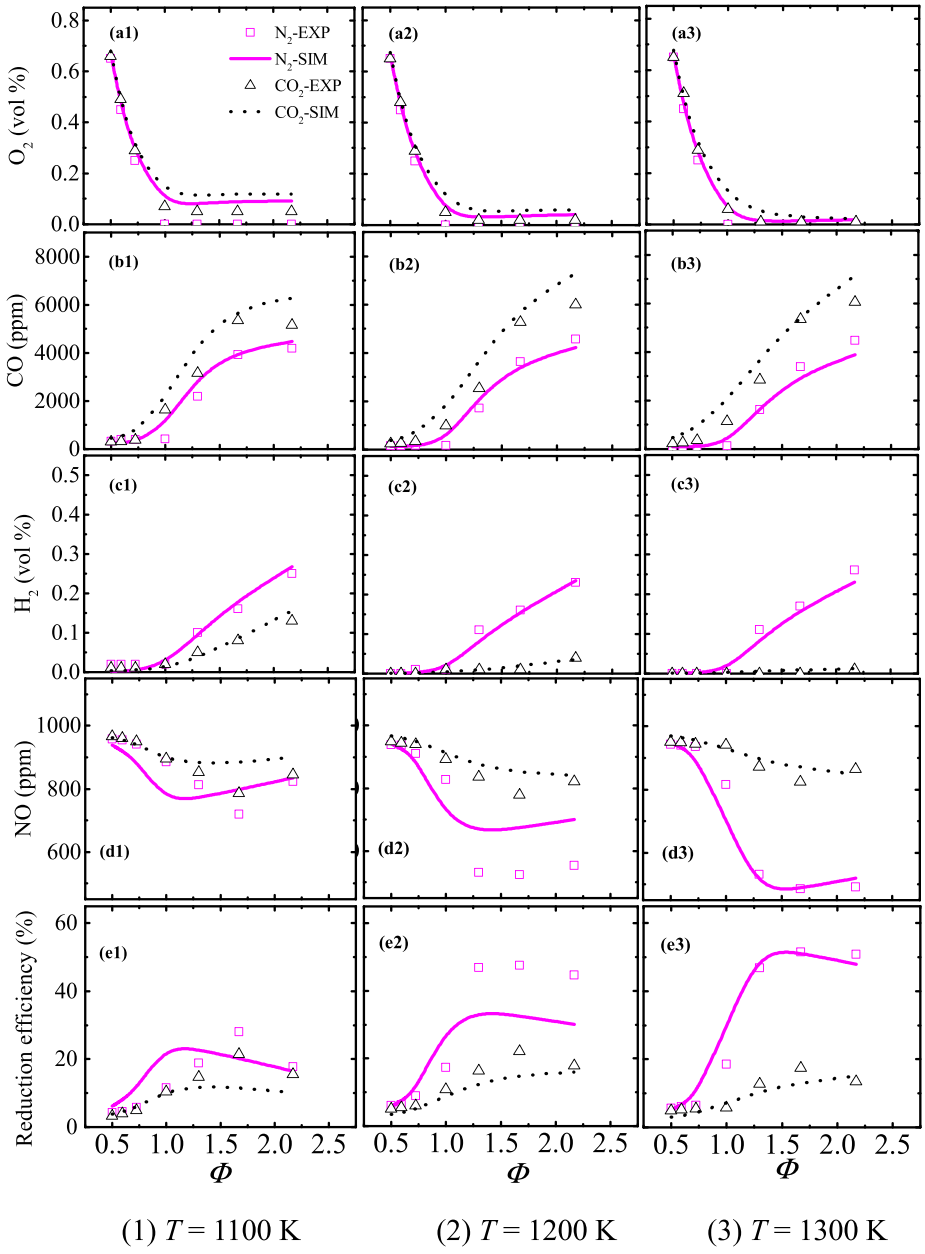

Fig. 10. Experimental and simulated results of O_2, CO, H_2, NO concentrations and NO reduction efficiencies with different Φ under three T with addition of methane.

efficiency with dependency on Φ with the addition of methane at three temperatures. The variation trends of NO and the reduction efficiency are similar with the results in Fig. 5d & 5e at the three temperatures under both the N_2 and CO_2 conditions. However, the maximum decreases of NO and reduction efficiencies are all larger than the corresponding reaction conditions in Fig. 5d & 5e. Under the N_2 condition, the maximum NO reduction efficiency is about 52% and is increased by 79% compared with the results in Fig. 5e. Under the CO_2 condition, the maximum NO reduction efficiency in Fig. 11e is approximately 22%, which is significantly improved than the results without CH_4 addition in Fig. 5e by approximately 267%.

Combining the results in Fig. 3b, 5e, 8b, 9e, and 10e, the NO-reburning by syngas can be remarkably inhibited by the presence of CO_2, while it can be significantly enhanced by the addition of 1000 ppm methane regardless of the variations of T, Φ and α. More importantly, the optimal condition for NO-reburning by syngas with the presence of both CO_2 and CH_4 is $T \approx 1150$ K, $\Phi \approx 1.67$ and $\alpha \approx 1$.

The pathways of NO reduction by syngas with methane addition are carried out under the fuel-rich condition at 1300 K in both (a) N_2 and (b) CO_2 atmospheres are demonstrated in Fig. 11. It can be found that the presence of CH_4 makes the pathway of NO reduction stronger and more complex than that in Fig. 7, resulting from the addition of CH_4 generating CH_3, CH_2 and HCCO radicals in the reaction process. The addition of CH_x radicals, which are the most critical radicals for NO reduction [46,47,74], makes the NO reduction pathway more intense and complicated, and also significantly enhances the NO reduction. Therefore, the overall reaction rates of NO reduction reaction in Fig. 11 are significantly greater than that in Fig. 7 without methane addition. Consequently, the addition of methane can significantly improve the NO-reburning by syngas in both N_2 and CO_2 atmospheres.

For N_2 atmosphere in Fig. 11a, the NO reduction by syngas with methane addition is mainly through the paths of NO → HNCO → NH_2 → NNH → N_2 and NO → HCNO/H_2CN → HCN → NH/NCO → N_2. While for CO_2 atmosphere in Fig. 11b, the overall reaction rate of NO reduction reaction is lower than that in N_2 atmosphere, and the values of related reaction rate are decreased by one order of magnitude. In particular, the

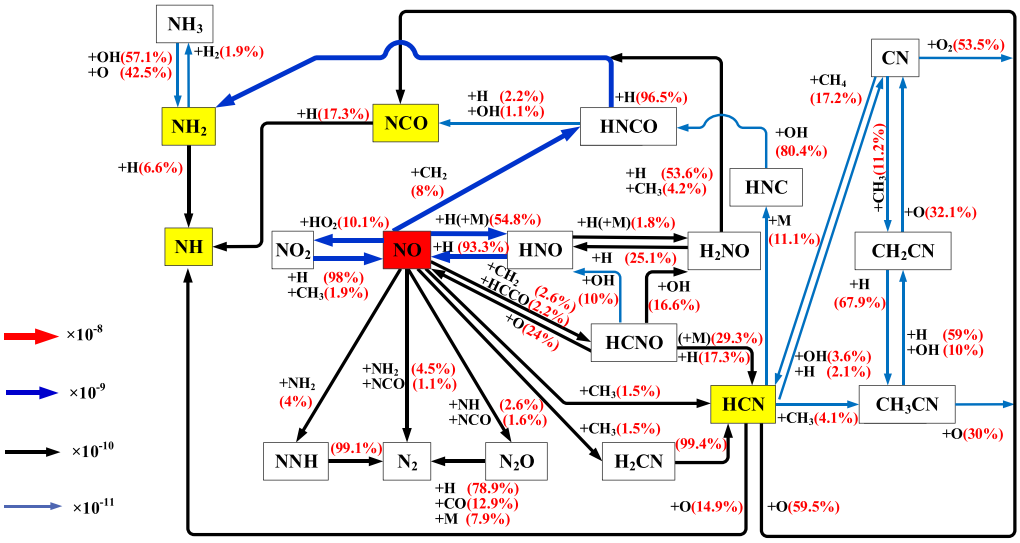

(a) N_2 condition (T = 1300 K, Φ = 1.67, X_{CO} = 4500 ppm, X_{H2} = 4500 ppm, X_{CH4} = 1000 ppm, and X_{NO} = 1000 ppm)

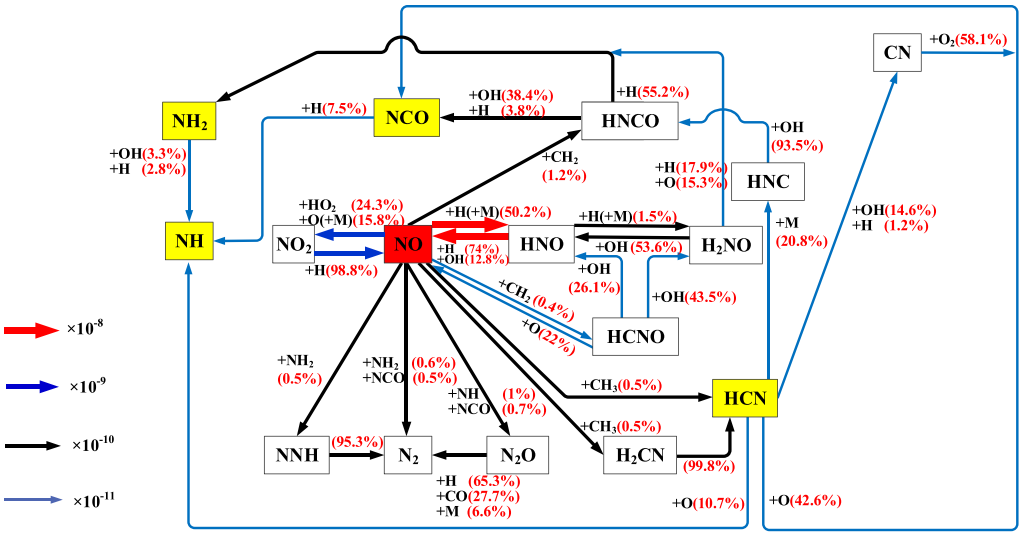

(b) CO_2 condition (T = 1300 K, Φ = 1.67, X_{CO} = 4500 ppm, X_{H2} = 4500 ppm, X_{CH4} = 1000 ppm, X_{NO} = 1000 ppm, and X_{CO2} = 0.30)

Fig. 11. Reaction pathways of NO reduction by syngas with addition of methane under (a) N_2 and (b) CO_2 conditions.

reaction path of NO → HNCO → NH_2 → NNH → N_2 is dramatically inhibited. The conversion of NO to NO_2 is enhanced, 40.1% of NO is converted to NO_2 and then to NO, which is higher than the 10.1% in N_2 atmosphere. The reaction rate of NO to HNO is increased by an order of magnitude in comparison to that in N_2 atmosphere. Therefore, the NO reduction of syngas with methane addition in CO_2 atmosphere is observably reduced in comparison to that in N_2 atmosphere.

The first-order sensitivity analysis for NO of syngas with CH_4 in N_2 and CO_2 atmospheres is shown in Fig. 12. Under the N_2 condition, the top four crucial reactions to promote NO reduction are $CH_2 + NO \leftrightarrow H + HNCO$, $CH_2(S) + H_2 \leftrightarrow CH_3 + H$, $O + H_2 \leftrightarrow OH + H$, $H + O_2 \leftrightarrow O + OH$. The last two reactions are the main chain branching reactions during the combustion process, which contributes to the formation of CH_x radicals, while the first two reactions are the initial reactions of NO reduction. Under the CO_2 atmosphere, these four vital reactions are strongly inhibited, and thus the NO-reburning is significantly reduced. More importantly, the elementary reactions, i.e., $CH_3 + H (+M) \leftrightarrow CH_4 (+M)$, $HNO + H \leftrightarrow NO + H_2$, $H + O_2 \leftrightarrow O + OH$, $CH_3 + NO \leftrightarrow HCN + H_2O$, and $CH_3 + NO \leftrightarrow H_2CN + OH$, are found to be important and required attention for future mechanism development and application of the NO-reburning by syngas in the presence of CH_4 and CO_2.

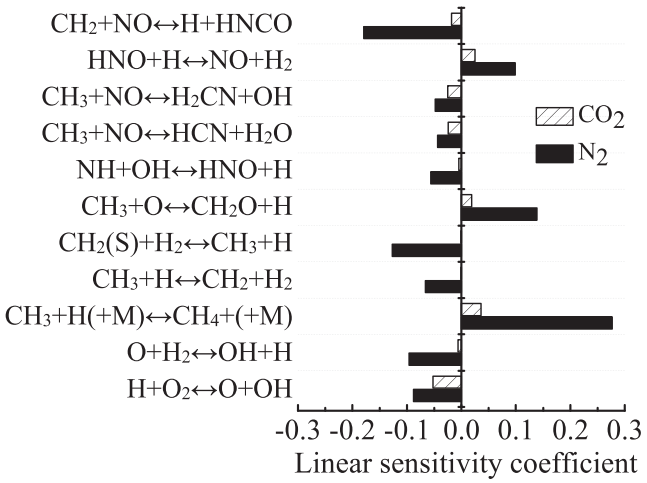

Fig. 12. First-order sensitivity analysis for NO of syngas with CH_4 under N_2 and CO_2 atmospheres.

5. Conclusions

The present study experimentally and numerically investigates the NO-reburning by syngas in a jet-stirred reactor (JSR). The effects of CO_2 and methane are systematically studied under various reaction temperatures (T), equivalence ratios (Φ) and initial ratios of hydrogen to carbon monoxide (α). The main conclusions are as follows:

(1) For the syngas without CH_4, the presence of CO_2 can significantly inhibit the NO-reburning, regardless of the variation of T, Φ and α. The NO reduction efficiency is<10% under fuel-lean and stoichiometric conditions no matter for N_2 or CO_2 atmospheres. Under fuel-rich conditions, the maximum reduction efficiency under the CO_2 condition is lower than that under the N_2 condition by at least 76%.

(2) The addition of 1000 ppm methane can obviously increase the NO-reburning by syngas under CO_2 conditions by at least 243%. Because actual syngas contains CH_4, its effect on NO-reburning by syngas must be taken into account. The NO-reburning by syngas with the presence of CO_2 and CH_4 can be operated at the optimal condition, i.e., $T \approx 1150$ K, $\Phi \approx 1.67$, and $\alpha \approx 1$ to achieve the maximum reburning efficiency.

(3) The present modified mechanism for NO-reburing by syngas is updated and validated, especially for simulating NO-reburning under high CO_2 concentration conditions. The modeling using the present mechanism has good consistency with our experiments under most conditions in both N_2 and CO_2 atmospheres.

(4) Pathway analysis confirms that the main pathways for NO reduction by syngas are NO → HNO → H_2NO → NH_2 (→NNH) → N_2 and NO → HNO → NH → N_2O → N_2, and the former path is dramatically inhibited under CO_2 condition. The critical pathways for NO reduction by syngas with methane addition are NO → HNCO → NH_2 → NNH → N_2 and NO → HCNO/H_2CN → HCN → NH/NCO → N_2, and the former path is significantly weakened in CO_2 atmosphere.

(5) Important reactions, i.e., $CH_3 + H (+M) \leftrightarrow CH_4 (+M)$, $HNO + H \leftrightarrow NO + H_2$, $H + O_2 \leftrightarrow O + OH$, $CH_3 + NO \leftrightarrow HCN + H_2O$, and $CH_3 + NO \leftrightarrow H_2CN + OH$, are identified for future development of the NO-reburning mechanism by syngas in the presence of CH_4 and CO_2.

CRediT authorship contribution statement

Fan Hu: Methodology, Investigation, Formal analysis, Data curation, Visualization, Writing - original draft, Writing - review & editing. **Pengfei Li:** Methodology, Formal analysis, Funding acquisition, Resources, Supervision, Writing - original draft, Writing - review & editing. **Wenhao Li:** Investigation, Data curation. **Cuijiao Ding:** Methodology, Formal analysis. **Junjun Guo:** Methodology, Formal analysis. **Zhaohui Liu:** Methodology, Formal analysis, Funding acquisition, Resources, Supervision.

Declaration of Competing Interest

The authors declare that they have no known competing financial interests or personal relationships that could have appeared to influence the work reported in this paper.

Acknowledgment

This work is supported by the National Natural Science Foundation of China (52076095 and 51906075), the National Key Research and Development Program of China (2019YFE0100100), the China Postdoctoral Science Foundation (2020M672349), Young Elite Scientists Sponsorship Program by CAST (2018QNRC001), and the China Coal Technology and Engineering Group (2018-TD-QN006).

Appendix A. Supplementary data

Supplementary data to this article can be found online at https://doi.org/10.1016/j.fuel.2021.121403.

References

[1] Zhu S, Lyu Q, Zhu J, Wu H, Wu G. Effect of Air Distribution on NO_x Emissions of Pulverized Coal and Char Combustion Preheated by a Circulating Fluidized Bed. Energ Fuels 2018;32(7):7909–15.
[2] Ali G, Zhang T, Wu W, Zhou Y. Effect of hydrogen addition on NO_x formation mechanism and pathways in MILD combustion of H_2-rich low calorific value fuels. Int J Hydrogen Energy 2020;45(15):9200–10.
[3] Smoot LD, Hill S, Xu H. NO_x control through reburning. Prog Energy Combust Sci 1998;24(5):385–408.
[4] Oluwoye I, Altarawneh M, Gore J, Dlugogorski BZ. Products of incomplete combustion from biomass reburning. Fuel 2020;274:117805. https://doi.org/10.1016/j.fuel.2020.117805.
[5] Oluwoye I, Zeng Z, Mosallanejad S, Altarawneh M, Gore J, Dlugogorski BZ. Controlling NO_x emission from boilers using waste polyethylene as reburning fuel. Chem Eng J 2021;411:128427. https://doi.org/10.1016/j.cej.2021.128427.
[6] Sahu AB, Ravikrishna RV. Quantitative LIF measurements and kinetics assessment of NO formation in H_2/CO syngas–air counterflow diffusion flames. Combust Flame 2016;173:208–28.
[7] Pio G, Ricca A, Palma V, Salzano E. Experimental and numerical evaluation of low-temperature combustion of bio-syngas. Int J Hydrogen Energy 2020;45(1):1084–95.
[8] Glarborg P, Kristensen PG, Dam-Johansen K, Alzueta MU, Millera A, Bilbao R. Nitric oxide reduction by non-hydrocarbon fuels. Implications for reburning with gasification gases. Energ Fuels 2000;14(4):828–38.
[9] Dagaut P, Lecomte F. Experiments and kinetic modeling study of NO-reburning by gases from biomass pyrolysis in a JSR. Energ Fuels 2003;17(3):608–13.
[10] Werle S. Modeling of the reburning process using sewage sludge-derived syngas. Waste Manag 2012;32(4):753–8.
[11] Nazeer WA, Jackson RE, Peart JA, Tree DR. Detailed measurements in a pulverized coal flame with natural gas reburning. Fuel 1999;78(6):689–99.
[12] Han SH, Chang D, Yang W. Numerical study on the reburning characteristics of biomass syngas in a 2 MW pilot scale heavy oil furnace. Fuel 2016;181:277–85.
[13] Ślefarski R, Jójka J, Czyżewski P, Grzymisławski P. Experimental investigation on syngas reburning process in a gaseous fuel firing semi-idustrial combustion chamber. Fuel 2018;217:490–8.
[14] Yang W, Yang DJ, Choi SY, Kim JS. Experimental Study on Co-Firing of Syngas as a Reburn/Alternative Fuel in a Commercial Water-Tube Boiler and a Pilot-Scale Vertical Furnace. Energ Fuels 2011;25(6):2460–8.
[15] Zhao J, Wang Q, Yu L, Wu L. Influence of the biogas reburning for reducing nitric oxide emissions in an alundum-tube reactor. Atmos Environ 2016;132:290–5.
[16] Zhou Q, Cheung CS, Leung CW, Li X, Li X, Huang Z. Effects of fuel composition and initial pressure on laminar flame speed of H_2/CO/CH_4 bio-syngas. Fuel 2019;238:149–58.
[17] Fürst M, Sabia P, Lubrano Lavadera M, Aversano G, de Joannon M, Frassoldati A, et al. Optimization of Chemical Kinetics for Methane and Biomass Pyrolysis Products in Moderate or Intense Low-Oxygen Dilution Combustion. Energ Fuels 2018;32(10):10194–201.

[18] Voss S, Hartl S, Hasse C. Determination of laminar burning velocities for lean low calorific H_2 /N_2 and H_2 /CO/N_2 gas mixtures. Int J Hydrogen Energy 2014;39(34):19810–7.

[19] Sahu AB, Ravikrishna RV. Effect of H_2/CO Composition on Extinction Strain Rates of Counterflow Syngas Flames. Energ Fuels 2015;29(7):4586–96.

[20] Huang M, Deng H, Liu Y, Zhang B, Cheng S, Zhang X, et al. Effect of fuel type on the MILD combustion of syngas. Fuel 2020;281:118509. https://doi.org/10.1016/j.fuel.2020.118509.

[21] Mathieu O, Kopp MM, Petersen EL. Shock-tube study of the ignition of multi-component syngas mixtures with and without ammonia impurities. Proc Combust Inst 2013;34(2):3211–8.

[22] Wang J, Huang Z, Kobayashi H, Ogami Y. Laminar burning velocities and flame characteristics of CO–H_2–CO_2–O_2 mixtures. Int J Hydrogen Energy 2012;37(24):19158–67.

[23] Wang Z, Zhou Y, Whiddon R, He Y, Cen K, Li Z. Investigation of NO formation in premixed adiabatic laminar flames of H_2 /CO syngas and air by saturated laser-induced fluorescence and kinetic modeling. Combust Flame 2016;164:283–93.

[24] Dagaut P, Luche J, Cathonnet M. The kinetics of C1 to C4 hydrocarbons/no interactions in relation with reburning. Proc Combust Inst 2000;28(2):2459–65.

[25] DAGAUT P, DAYMA G. The high-pressure reduction of nitric oxide by a natural gas blend. Combust Flame 2005;143(1-2):135–7.

[26] Dagaut P, Luche J, Cathonnet M. Experimental and kinetic modeling of the reduction of NO by propene at 1 atm. Combust Flame 2000;121(4):651–61.

[27] Bilbao R, Millera A, Alzueta MU. Influence of the Temperature and Oxygen Concentration on NO_x Reduction In The Natural Gas Reburning Process. Ind Eng Chem Res 1994;33(11):2846–52.

[28] Do H-S, Tran T-S, Han Z, Zeng Xi, Gao S, Xu G. Synergetic NO reduction by biomass pyrolysis products simulating their reburning in circulating fluidized bed decoupling combustion. Chinese J Chem Eng 2019;27(7):1680–9.

[29] Nicolle A, Dagaut P. Occurrence of NO-reburning in MILD combustion evidenced via chemical kinetic modeling. Fuel 2006;85(17-18):2469–78.

[30] Liesa F, Alzueta MU, Millera A, Bilbao R. Influence of Reactant Mixing in a Laminar Flow Reactor: The Case of Gas Reburning. 1. Experimental Study. Ind Eng Chem Res 2007;46(11):3520-7.

[31] Wang E, Zhang M. Experimental Study on the Influences of the Water Vapor for the Methane Reburning Process. Energy Fuels 2012;26(6):3212–7.

[32] Giménez-López J, Aranda V, Millera A, Bilbao R, Alzueta MU. An experimental parametric study of gas reburning under conditions of interest for oxy-fuel combustion. Fuel Process Technol 2011;92(3):582–9.

[33] Shu Y, Zhang F, Wang H, Zhu J, Tian G, Zhang C, et al. An experimental study of NO reduction by biomass reburning and the characterization of its pyrolysis gases. Fuel 2015;139:321–7.

[34] Jiang K, Ashworth P. The development of Carbon Capture Utilization and Storage (CCUS) research in China: A bibliometric perspective. Renew Sust Energ Rev 2021;138:110521. https://doi.org/10.1016/j.rser.2020.110521.

[35] Naik SP, Ryu T, Bui Vy, Miller JD, Drinnan NB, Zmierczak W. Synthesis of DME from CO_2/H_2 gas mixture. Chem Eng J 2011;167(1):362–8.

[36] Bachu S. Identification of oil reservoirs suitable for CO_2-EOR and CO_2 storage (CCUS) using reserves databases, with application to Alberta. Canada. Int J Greenh Gas Control 2016;44:152–65.

[37] Sepehri A, Sarrafzadeh M-H, Avateffazeli M. Interaction between Chlorella vulgaris and nitrifying-enriched activated sludge in the treatment of wastewater with low C/N ratio. J Clean Prod 2020;247:119164. https://doi.org/10.1016/j.jclepro.2019.119164.

[38] Sepehri A, Sarrafzadeh M-H. Activity enhancement of ammonia-oxidizing bacteria and nitrite-oxidizing bacteria in activated sludge process: metabolite reduction and CO_2 mitigation intensification process. App Water Sci 2019;9(5):131.

[39] Chen Z, Fang J, Xu C, Xia Z, Yan K, Li X. Carbon dioxide hydrate separation from Integrated Gasification Combined Cycle (IGCC) syngas by a novel hydrate heat-mass coupling method. Energy 2020;199:117420. https://doi.org/10.1016/j.energy.2020.117420.

[40] Bravo J, Drapanauskaite D, Sarunac N, Romero C, Jesikiewicz T, Baltrusaitis J. Optimization of energy requirements for CO_2 post-combustion capture process through advanced thermal integration. Fuel 2021;283:118940. https://doi.org/10.1016/j.fuel.2020.118940.

[41] Zheng C, Liu Z. Oxy-fuel Combustion: Fundamentals. Theory and Practice: Academic Press; 2017.

[42] Chen L, Yong SZ, Ghoniem AF. Oxy-fuel combustion of pulverized coal: Characterization, fundamentals, stabilization and CFD modeling. Prog Energy Combust Sci 2012;38(2):156–214.

[43] Guo J, Liu Z, Huang X, Zhang T, Luo W, Hu F, et al. Experimental and numerical investigations on oxy-coal combustion in a 35MW large pilot boiler. Fuel 2017;187:315–27.

[44] Normann F, Andersson K, Leckner Bo, Johnsson F. Emission control of nitrogen oxides in the oxy-fuel process. Prog Energy Combust Sci 2009;35(5):385–97.

[45] Li P, Li W, Wang K, Hu F, Ding C, Guo J, et al. Experiments and kinetic modeling of NO reburning by CH_4 under high CO_2 concentration in a jet-stirred reactor. Fuel 2020;270:117476. https://doi.org/10.1016/j.fuel.2020.117476.

[46] Mendiara T, Glarborg P. Reburn Chemistry in Oxy-fuel Combustion of Methane. Energ Fuels 2009;23(7):3565–72.

[47] He Y, Luo J, Li Y, Jia H, Wang F, Zou C, et al. Comparison of the Reburning Chemistry in O_2/N_2, O_2/CO_2, and O_2/H_2O Atmospheres. Energ Fuels 2017;31(10):11404–12.

[48] Normann F, Andersson K, Johnsson F, Leckner Bo. Reburning in oxy-fuel combustion: a parametric study of the combustion chemistry. Ind Eng Chem Res 2010;49(19):9088–94.

[49] Kühnemuth D, Normann F, Andersson K, Johnsson F, Leckner Bo. Reburning of Nitric Oxide in Oxy-Fuel Firing—The Influence of Combustion Conditions. Energ Fuels 2011;25(2):624–31.

[50] Lubrano Lavadera M, Sabia P, de Joannon M, Cavaliere A, Ragucci R. Propane oxidation in a Jet Stirred Flow Reactor. The effect of H_2O as diluent species. Exp Therm Fluid Sci 2018;95:35–43.

[51] DAGAUT P, NICOLLE A. Experimental study and detailed kinetic modeling of the effect of exhaust gas on fuel combustion: mutual sensitization of the oxidation of nitric oxide and methane over extended temperature and pressure ranges. Combust Flame 2005;140(3):161–71.

[52] David R, Matras D. Rules for construction and extrapolation of reactors self-stirred by gas jets. Can J Chem Eng 1975;53:297–300.

[53] Glarborg P, Kee RJ, Grcar JF, Miller JA. PSR: A Fortran Program for Modeling Well-Stirred Reactors. Sandia National Laboratories Report, SAND86-8209; 1986.

[54] Glarborg P, Miller JA, Ruscic B, Klippenstein SJ. Modeling nitrogen chemistry in combustion. Prog Energy Combust Sci 2018;67:31–68.

[55] Smith GP, Golden DM, Frenklach M, Moriarty NW, Eiteneer B, Goldenberg M, et al. GRI-Mech 3.0, Available from: http://combustion.berkeley.edu/gri-mech/version30/text30.html; 1999.

[56] Bowman CT, Hanson, R. K., Davidson, D. F., Gardiner, Jr. W. C., Lissianski, V., Smith, G. P., Golden, D. M., Frenklach, M., Goldenberg, M. GRI-Mech 2.11, http://www.me.berkeley.edu/gri_mech/. 1995.

[57] Konnov AA. Implementation of the NCN pathway of prompt-NO formation in the detailed reaction mechanism. Combust Flame 2009;156(11):2093–105.

[58] Mendiara T, Glarborg P. Ammonia chemistry in oxy-fuel combustion of methane. Combust Flame 2009;156(10):1937–49.

[59] CRECK. C1C3HT_NOX_1412 kinetic mechanism, Detailed mechanism of the pyrolysis, partial oxidation and combustion of hydrocarbon fuels up to 3 C atoms with NOx, http://creckmodeling.chem.polimi.it/menu-kinetics/menu-kinetics-detailed mechanisms/menu-kinetics-c1-c3-mechanism. 2014.

[60] Wang H, You X, Joshi AV, Davis SG, Laskin A, Egolfopoulos F, et al. USC Mech Version II. High-Temperature Combustion Reaction Model of H2 /CO /C1–C4 Compounds; 2007.

[61] You X, Wang H, Goos E, Sung C-J, Klippenstein SJ. Reaction kinetics of CO+HO2→products: ab initio transition state theory study with master equation modeling. J Phys Chem A 2007;111(19):4031-42.

[62] Joshi AV, Wang H. Master equation modeling of wide range temperature and pressure dependence of CO+ OH→ products. Int J Chem Kinet 2006;38(1):57–73.

[63] Mackie JC, Bacskay GB. Quantum Chemical Study of the Mechanism of Reaction between NH ($X\ ^3\Sigma$-) and H_2, H_2O, and CO_2 under Combustion Conditions. J Phys Chem A 2005;109(51):11967–74.

[64] Wooldridge MS, Hanson RK, Bowman CT. A shock tube study of CO+OH→CO_2+H and HNCO+OH→products via simultaneous laser absorption measurements of OH and CO_2. Int J Chem Kinet 1996;28(5):361–72.

[65] Metcalfe WK, Burke SM, Ahmed SS, Curran HJ. A hierarchical and comparative kinetic modeling study of C1–C2 hydrocarbon and oxygenated fuels. Int J Chem Kinet 2013;45(10):638–75.

[66] Fomin A, Zavlev T, Alekseev VA, Rahinov I, Cheskis S, Konnov AA. Experimental and modelling study of $1CH_2$ in premixed very rich methane flames. Combust Flame 2016;171:198–210.

[67] Jodkowski JT, Ratajczak E, Sillesen A, Pagsberg P. Kinetics of the addition reaction of methyl radicals with nitric oxide studied by pulse radiolysis combined with infrared diode laser spectroscopy. Chem Phys Lett 1993;203(5-6):490–6.

[68] Atkinson R, Baulch DL, Cox RA, Hampson RF, Kerr JA, Rossi MJ, et al. Evaluated kinetic and photochemical data for atmospheric chemistry: supplement VI. IUPAC subcommittee on gas kinetic data evaluation for atmospheric chemistry. J Phys Chem Ref Data 1997;26(6):1329–499.

[69] Faravelli T, Frassoldati A, Ranzi E. Kinetic modeling of the interactions between NO and hydrocarbons in the oxidation of hydrocarbons at low temperatures. Combust Flame 2003;132(1–2):188–207.

[70] Atakan B, Kocis D, Wolfrum J, Nelson P. Direct investigations of the kinetics of the reactions of CN radicals with N atoms and $3CH_2$ radicals with NO. Symp (Intern) Combust 1992;24(1):691–9.

[71] Klippenstein SJ, Harding LB, Glarborg P, Miller JA. The role of NNH in NO formation and control. Combust Flame 2011;158(4):774–89.

[72] Hu F, Li P, Guo J, Wang K, Liu Z, Zheng C. Evaluation, development, and validation of a new reduced mechanism for methane oxy-fuel combustion. Int J Greenh Gas Control 2018;78:327–40.

[73] Hu F, Li P, Wang K, Li W, Guo J, Liu Lu, et al. Evaluation, development, and application of a new skeletal mechanism for fuel-NO formation under air and oxy-fuel combustion. Fuel Process Technol 2020;199:106256. https://doi.org/10.1016/j.fuproc.2019.106256.

[74] Normann F, Andersson K, Johnsson F, Leckner Bo. NO_x reburning in oxy-fuel combustion: A comparison between solid and gaseous fuels. Int J Greenh Gas Control 2011;5:S120–6.